In vivo photoacoustic tomography of total blood flow and Doppler angle

Junjie Yao, Konstantin I. Maslov, Lihong V. Wang

Junjie Yao, Konstantin I. Maslov, Lihong V. Wang, "In vivo photoacoustic tomography of total blood flow and Doppler angle," Proc. SPIE 8223, Photons Plus Ultrasound: Imaging and Sensing 2012, 82230U (23 February 2012); doi: 10.1117/12.909480

SPIE.

Event: SPIE BiOS, 2012, San Francisco, California, United States

In Vivo Photoacoustic Tomography of Total Blood Flow and Doppler Angle

Junjie Yao, Konstantin I. Maslov, Lihong V. Wang*

Department of Biomedical Engineering, Washington University in St. Louis,

St. Louis, MO 63130, USA

*Corresponding author: lhwang@biomed.wustl.edu

Abstract

As two hallmarks of cancer, angiogenesis and hypermetabolism are closely related to increased blood flow. Volumetric blood flow measurement is important to understanding the tumor microenvironment and developing new means to treat cancer. Current photoacoustic blood flow estimation methods focus on either the axial or transverse component of the flow vector. Here, we propose a method to compute the total flow speed and Doppler angle by combining the axial and transverse flow measurements. Both the components are measured in *M*-mode. Collating the A-lines side by side yields a 2D matrix. The columns are Hilbert transformed to compare the phases for the computation of the axial flow. The rows are Fourier transformed to quantify the bandwidth for the computation of the transverse flow. From the axial and transverse flow components, the total flow speed and Doppler angle can be derived. The method has been verified by flowing bovine blood in a plastic tube at various speeds from 0 to 7.5 mm/s and at Doppler angles from 30 to 330º. The measurement error for total flow speed was experimentally determined to be less than 0.3 mm/s; for the Doppler angle, it was less than 15°. In addition, the method was tested *in vivo* on a mouse ear. The advantage of this method is simplicity: No system modification or additional data acquisition is required to use our existing system. We believe that the proposed method has the potential to be used for cancer angiogenesis and hypermetabolism imaging.

Keywords: photoacoustic tomography, blood flow, transverse flow, axial flow, total flow, Doppler angle

Introduction

As photoacoustic tomography has becoming an important imaging modality for biomedical applications [1-9], blood flow measurement by photoacoustic method is attracting more and more attentions due to the excellent contrast provided by the hemoglobin. So far, photoacoustic flow measurements have focused on either the axial [10-13] or transverse [3, 14-16] component of the flow vector. However, to quantify the total flow vector, the Doppler angle (angle of the flow direction relative to the axis of the received acoustic wave) is needed. The Doppler angle can be estimated by tracing the vessel centerline either manually or automatically in a volumetric image [17, 18]. In practice, however, volumetric information is not always available, as in the case of *M*-mode imaging. In addition, despite the additional time required for volumetric imaging, accurate estimation of the Doppler angle is challenging if the system's axial and lateral resolutions do not match. Here, using PAM, we propose a simple method for measuring total flow and the Doppler angle by combining the axial and transverse flow measurements. Briefly, the axial flow speed is estimated from the phase shift between consecutive Hilbert transformed pairs of A-lines. The sign of the phase shift provides the axial flow direction. The transverse flow speed is quantified from the bandwidth broadening via the Fourier transformation of sequential A-lines. The transverse flow direction can be measured by bi-directional scanning.

Theory and methods

Inspired by previous work in ultrasound imaging [19] and optical coherence tomography [20], we use the following formula to compute the axial component v_a pixelwise:

Photons Plus Ultrasound: Imaging and Sensing 2012, edited by Alexander A. Oraevsky, Lihong V. Wang,
Proc. of SPIE Vol. 8223, 82230U · © 2012 SPIE · CCC code: 1605-7422/12/$18 · doi: 10.1117/12.909480

$$v_a = \frac{1}{2\pi} \cdot \frac{c}{T} \cdot \frac{\Delta\phi}{f_0}, \quad [1]$$

where c is the speed of sound in water (1500 m/s), T is the time interval between the two consecutive A-lines acquired in *M*-mode, $\Delta\phi$ is the phase shift in each pixel between two consecutive A-lines, and f_0 is the central frequency of an ultrasonic transducer. The phase shift $\Delta\phi$ is quantified via the Hilbert transformation. The sign of $\Delta\phi$ provides the axial flow direction, where positive $\Delta\phi$ means a flow towards the ultrasonic transducer and vice versa. The axial flow velocity v_a is related to the total flow velocity v through $v \cdot \cos(\theta)$, where θ is the Doppler angle (Fig. 1).

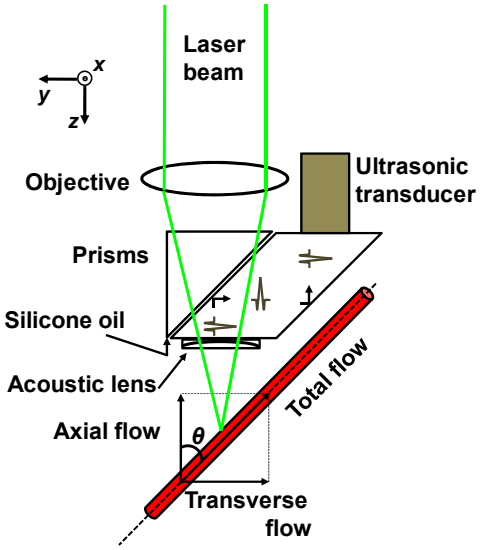

Figure 1. Schematic of the total flow measurement by photoacoustic microscopy. θ: Doppler angle.

It has also been demonstrated that the transverse flow component v_t, which equals $v \cdot \sin(\theta)$, can be estimated by

$$v_t = k \cdot \frac{B_d \cdot c \cdot F}{W \cdot f_0}, \quad [2]$$

where B_d is the bandwidth broadening, and F and W are the focal length and diameter of the ultrasonic transducer, respectively. k is an experimentally determined calibration factor. For a PAM system with confocal alignment but different optical and acoustic focal sizes, k mostly accounts for the discrepancy in the two foci. The transverse flow direction can be measured by bi-directional scanning, as long as the transverse flow is not perpendicular to the scanning line.

From the axial and transverse flow components, the Doppler angle θ can be derived as $\theta = \tan^{-1}(v_t / v_a)$, which ranges from 0° to 360°. The total flow speed v is computed by $v = \sqrt{v_a^2 + v_t^2}$.

The OR-PAM (Fig. 1) used in this study has a lateral resolution of ~5 μm, axial resolution of ~15 μm and penetration depth ~1.2 mm [5, 21]. A tunable dye laser (CBR-D, Sirah) pumped by a Nd:YLF laser (INNOSAB, Edgewave, 523 nm) was used as the excitation source. The short pulses (5 ns) from the dye laser were focused by a

microscope objective lens (Olympus 4×, NA=0.1) into the sample surface. Ultrasonic detection was achieved through a spherically focused ultrasonic transducer (V214-BC-RM, Panametrics-NDT, central frequency: 50 MHz), which was placed confocally with the objective. A ultrasound/light splitter, composed of a thin layer of silicone oil sandwiched between a right-angle prism and a rhomboid prism, was used for the co-axial alignment of the optical and acoustic beams [21]. A plano-convex lens was attached onto the top of the splitter to correct the refraction of the prisms. Distilled water was used as the matching medium for acoustic propagation. A motion controller provided trigger signals for laser firing, data acquisition, and raster scanning. While the lateral resolution of the system is defined by the diffraction-limited optical focus, the depth resolution is determined by the temporal resolution of the acoustic detection.

A laminar flow model was used to fit the flow speed profiles along the axial and transverse directions of the tube [22]:

$$v(x,z) = v_{\max}\left(1 - \frac{(x-x_0)^2 + (z-z_0)^2}{R^2}\right). \quad [3]$$

Here, x and z are the transverse and axial coordinates, respective, (x_0 , z_0) are the tube center coordinates, R is the tube radius, and $v_{\max}$ is the flow speed at the tube center. While (x_0 , z_0) and R can be measured directly from the cross-sectional image of the tube, $v_{\max}$ is the unknown parameter to be fitted for.

Flow phantom study

Defibrinated oxygenated bovine blood was used for the flow phantom. Two experiments were performed using this phantom. First, by changing the pumping speed, the mean flow speed was adjusted from 0 to 7.5 mm/s, with a step size of 0.25 mm/s, while the Doppler angle was fixed at 30º. Fig. 2(A) shows the measured mean axial, transverse, and total flow speeds as a function of the preset speeds. The speed measurement errors are less than 0.3 mm/s.

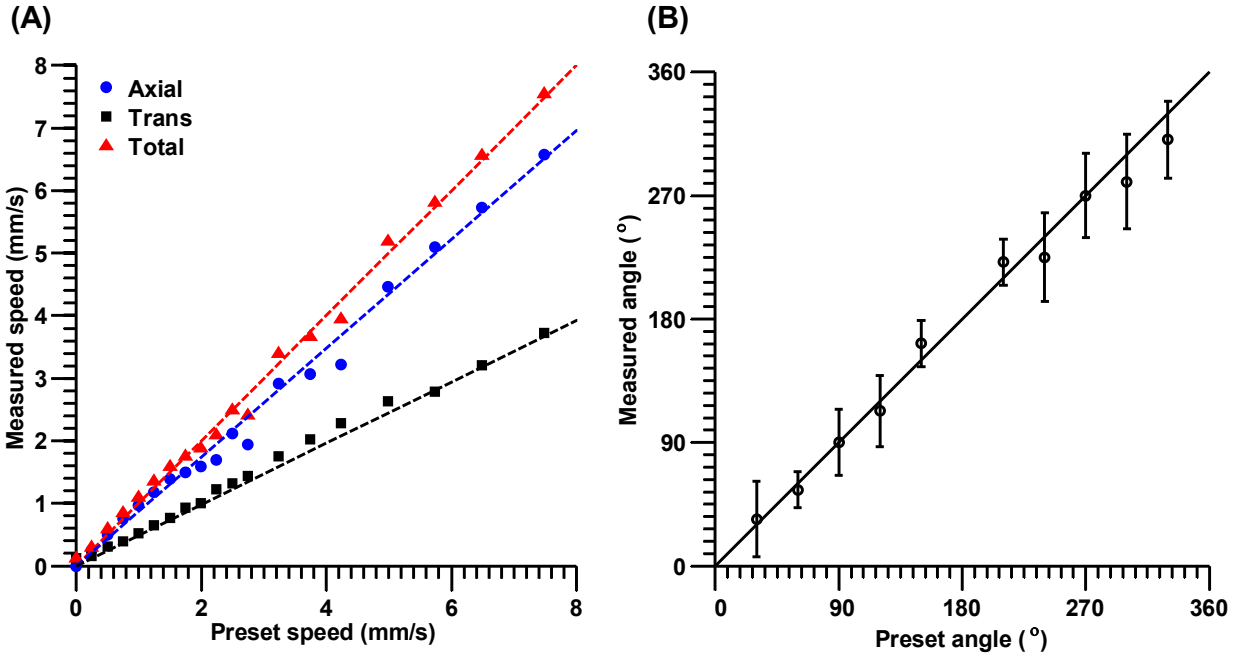

Figure 2. Total flow measurement on bovine blood flowing in a plastic tube (diameter: 200 μm). (A) Measured transverse, axial, total flow speeds versus the preset total flow speeds. (B) Measured Doppler angle as a function of the preset value. Error bars: standard deviations.

Second, by mounting the tube on a goniometer stage (GN05, Thorlabs), the Doppler angle was adjusted from 30º to 330º with a step size of 30º, while the mean total flow speed was fixed at 1.0 mm/s. The measured Doppler angles as a function of preset angles are shown in Fig. 2(B), which shows good agreement, within 15º.

In vivo study

The first experiment was performed on a stage-16 chicken embryo. For our study, since the chicken embryo has a relatively slow blood flow speed and heart beating rate, the time course of the blood flow can be sufficiently sampled without speed saturation. A chicken embryo was removed from a fertile white leghorn chicken egg (Sunrise Farms, Catskill, New York) after approximate 60 h of incubation and cultured in phosphate buffered saline (pH 7.0). The time course of the axial flow speed at the center of a vein was measured by using eight sequential A scans without motor scanning (Doppler angle 90°) [Figs. 3(A-B)]. The phase shift of PA signal between sequential A-lines and the heart beating pattern are clearly observed [Fig. 3(c)]. Infrared light was applied during the experiment to adjust the temperature (from 21°C to 39 °C) [Figs. 3(A-B)]. Compared with the measurements at 21°C, the peak flow speed increased from 1.0 mm/s to 3.0 mm/s at 39 °C and the heart beating rate increased from 0.8 Hz to 1.2 Hz.

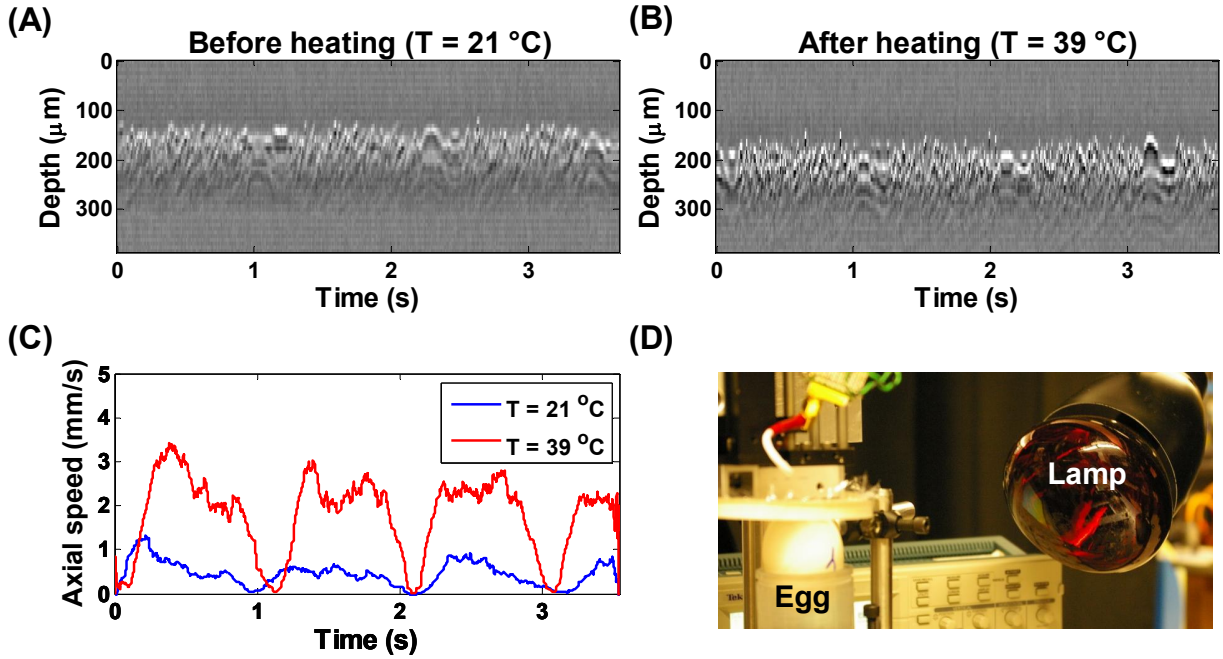

Figure 3. The flow speed measurement on a chicken embryo. (A-B) *M*-mode images of a vein at 21°C and 39°C. (C) The time courses of measured axial flow speeds at the two temperatures. (D) A photograph of the experimental setup.

The left ear of an adult, 6-week-old nude mouse (Hsd: Athymic Nude-Foxl^{NU}, Harlan Co.; body weight ~20 g) was also imaged *in vivo*. Several typical artery-vein pairs at the base of a nude mouse ear were imaged [Fig. 4]. The morphology indicates that the thicker vessels of the pairs are the veins, which was confirmed by the oxygen saturation image [Fig. 4(A)]. The volumetric rendering shows that the Doppler angles of the second artery and vein pair (A_2 and V_2) at the proximal ends were approximately 71.5º and 265.2º, respectively. The profile of total flow speed along the dashed line in Fig. 4(A) is shown in Fig. 4(B), where the arteries have faster flow than the veins. The total flow speeds at the centers of the artery A_2 and vein V_2 were 6.0 ± 0.15 mm/s and 2.5 ± 0.33 mm/s, respectively. The Doppler angles at the centers of the artery and vein were calculated as 70.0 ± 5.4º and 270.0 ± 1.8º, respectively, which were consistent with the measurements from the volumetric image.

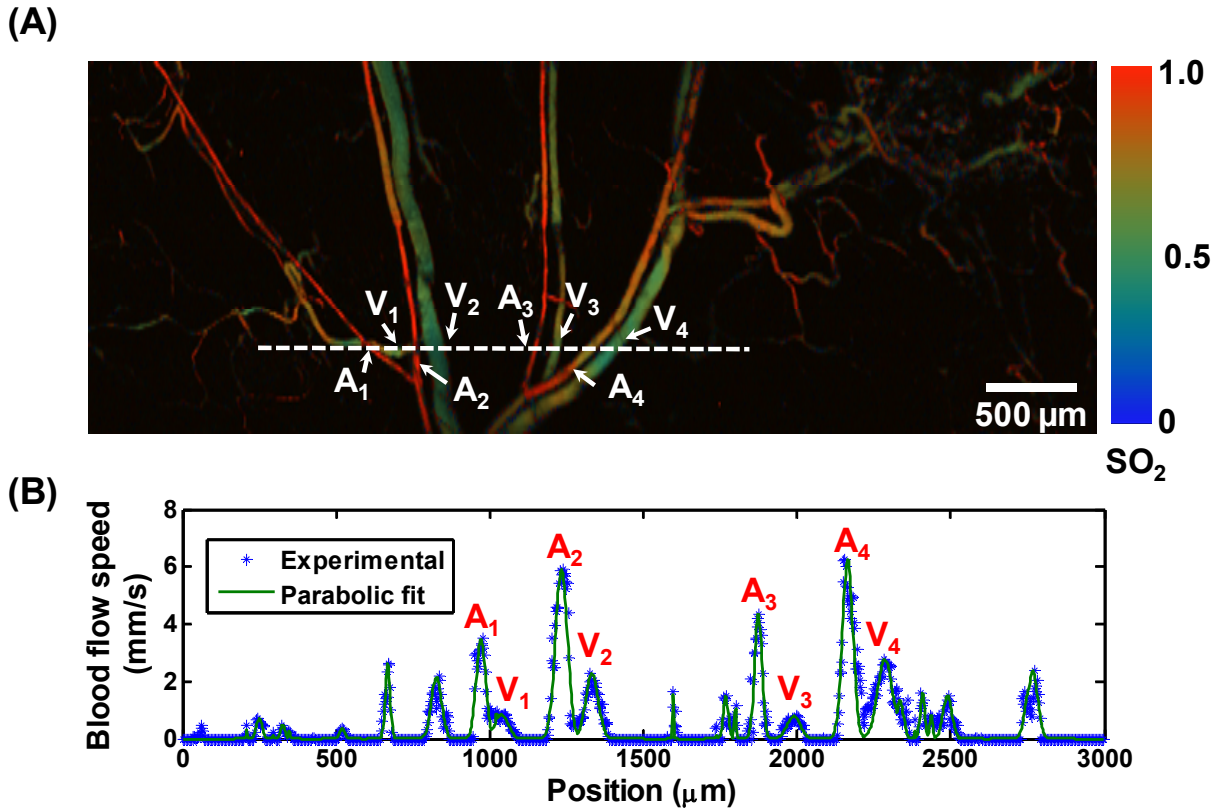

Figure 4. Multi-parametric PAM of a mouse ear. (A) sO_2 image of the four artery and vein pairs at the base of the ear. (B) Total flow speed profiles along the dashed line in (A).

Conclusions

We have demonstrated a method for measuring both total flow velocity without the Doppler angle and Doppler angle without the volumetric structural information by using PAM. By Combining blood flow information with other anatomical and functional parameters such as vessel cross-sections, C_{Hb} and sO_2, we can quantify the metabolic rate of oxygen (MRO_2) for cancer hypermetabolism studies.

Acknowledgements

The authors thank Christopher Favazza, Lidai Wang, and Arie Krumholz for helpful discussions, Zijian Guo for data processing. This research was supported by the National Institutes of Health Grants R01 EB000712, R01 EB008085, R01 CA134539, U54 CA136398, R01 EB010049, R01 CA157277, and 5P60 DK02057933. L.V.W. has a financial interest in Microphotoacoustics, Inc. and Endra, Inc., which, however, did not support this work.

References

[1] Yao, J. and Wang, L. V., "Photoacoustic tomography: fundamentals, advances and prospects," Contrast Media Mol Imaging. **6**(5), 332-45 (2011).

[2] Yao, J., et al., "Evans blue dye-enhanced capillary-resolution photoacoustic microscopy in vivo," Journal of Biomedical Optics. **14**(5), 054049 (2009).

[3] Yao, J., et al., "In vivo photoacoustic imaging of transverse blood flow by using Doppler broadening of bandwidth," Opt. Lett. **35**(9), 1419-1421 (2010).

[4] Yao, J., et al., "Label-free oxygen-metabolic photoacoustic microscopy in vivo," Journal of Biomedical Optics. **16**(7), 076003 (2011).

[5] Maslov, K., et al., "Optical-resolution photoacoustic microscopy for in vivo imaging of single capillaries," Optics Letters. **33**(9), 929-931 (2008).
[6] Wang, L., et al., "Fast voice-coil scanning optical-resolution photoacoustic microscopy," Opt Lett. **36**(2), 139-41 (2011).
[7] Wang, L. V., "Multiscale photoacoustic microscopy and computed tomography," Nature Photonics. **3**(9), 503-509 (2009).
[8] Zhang, C., Maslov, K., and Wang, L. V., "Subwavelength-resolution label-free photoacoustic microscopy of optical absorption in vivo," Opt Lett. **35**(19), 3195-7 (2010).
[9] Zhang, H. F., et al., "Functional photoacoustic microscopy for high-resolution and noninvasive in vivo imaging," Nature Biotechnology. **24**(7), 848-851 (2006).
[10] Sheinfeld, A., Gilead, S., and Eyal, A., "Photoacoustic Doppler measurement of flow using tone burst excitation," Optics Express. **18**(5), 4212-4221 (2010).
[11] Fang, H., Maslov, K., and Wang, L. V., "Photoacoustic Doppler effect from flowing small light-absorbing particles," Phys Rev Lett. **99**(18), 184501 (2007).
[12] Brunker, J. and Beard, P. *Pulsed photoacoustic Doppler flowmetry using a cross correlation method*. 2010. San Francisco, California, USA: SPIE.
[13] Sheinfeld, A., Gilead, S., and Eyal, A. *Time-resolved photoacoustic Doppler characterization of flow using pulsed excitation*. 2010. San Francisco, California, USA: SPIE.
[14] Fang, H. and Wang, L. H. V., "M-mode photoacoustic particle flow imaging," Optics Letters. **34**(5), 671-673 (2009).
[15] Chen, S. L., et al., "Photoacoustic correlation spectroscopy and its application to low-speed flow measurement," Optics Letters. **35**(8), 1200-2 (2010).
[16] Wei, C., et al., "Photoacoustic flow measurements based on wash-in analysis of gold nanorods," Ieee Transactions on Ultrasonics Ferroelectrics and Frequency Control. **54**(6), 1131-1141 (2007).
[17] King, D. L., King, D. L., Jr., and Shao, M. Y., "Three-dimensional spatial registration and interactive display of position and orientation of real-time ultrasound images," J Ultrasound Med. **9**(9), 525-32 (1990).
[18] Tola, M. and Yurdakul, M., "Effect of Doppler angle in diagnosis of internal carotid artery stenosis," J Ultrasound Med. **25**(9), 1187-92 (2006).
[19] Bonnefous, O. and Pesque, P., "Time Domain Formulation of Pulse-Doppler Ultrasound and Blood Velocity Estimation by Cross-Correlation," Ultrasonic Imaging. **8**(2), 73-85 (1986).
[20] Zhao, Y. H., et al., "Phase-resolved optical coherence tomography and optical Doppler tomography for imaging blood flow in human skin with fast scanning speed and high velocity sensitivity," Optics Letters. **25**(2), 114-116 (2000).
[21] Hu, S., Maslov, K., and Wang, L. V., "Second-generation optical-resolution photoacoustic microscopy with improved sensitivity and speed," Optics Letters. **36**(7), 1134-6 (2011).
[22] Cobbold, R. S. C., *Foundations of biomedical ultrasound*. Biomedical engineering series. 2007, New York: Oxford University Press. xix, 802 p.